Effects of initial packing density and cohesion on submerged granular collapse

Rui Zhu,[1,2] Zhiguo He,[2,*] and Eckart Meiburg[1,†]
[1]*Department of Mechanical Engineering, University of California at Santa Barbara, Santa Barbara, California 93106, USA*
[2]*Ocean College, Zhejiang University, Zhoushan 316021, China*

(Received 29 November 2023; accepted 22 July 2024; published 20 August 2024)

We investigate the collapse of submerged cohesive granular columns as a function of their packing density and the cohesive force strength, via grain-resolving direct numerical simulations. The cohesive force acts to reduce the final runout distance of the collapsing columns. In addition, it significantly accelerates the initial contraction for loosely packed columns and decelerates the dilation for densely packed columns, leading to a larger or smaller excess pore pressure, respectively. Early on, the collapsing column exhibits distinct planar failure surfaces, whose angle with the horizontal increases with the packing density. We employ a network science-based approach to analyze the cohesive and contact force chains. Pronounced force-chain network structures form preferentially in the failure region. They tend to be larger for higher packing density, which induces a larger macroscopic cohesive resistance. The cohesive force tends to reduce the normal contact force, which results in shorter contact force chains.

DOI: 10.1103/PhysRevFluids.9.084302

Submerged granular flows play a significant role in a wide range of industrial and environmental applications, where they are frequently associated with destructive behavior. A notable example is the large-scale turbidity current triggered by slope failure in the Grand Banks region of the northwest Atlantic Ocean in 1929, which caused damage to a series of submarine cables as far as 600 km away [1]. Previous studies found the dynamics of submerged granular flows to be strongly influenced by their packing density, due to the pore pressure feedback mechanism [2–4]. Cohesion among the smaller grains can furthermore lead to the formation and persistence of aggregates in such processes, which frequently play an important role for the transport of sediment in rivers, lakes, and estuaries [5–8].

The collapse of granular columns has long been employed as a canonical example for studying the dynamics of granular flows [9–18]. The influence of the initial packing density on submerged granular collapse was investigated both via experiments [19,20] and in numerical simulations [21,22]. Rondon *et al.* [19] and Yang *et al.* [22] observed that loosely packed columns undergo an initial contraction process, which leads to the development of positive excess pore pressure. This process reduces the interparticle contact and eventually causes a catastrophic failure. On the other hand, densely packed columns experience a dilation process, resulting in negative excess pore pressure. This process tends to enhance interparticle contact and prevent particle sliding. Rondon *et al.* [19] also found that the transition between the loosely and densely packed columns occurs near a critical packing density of 0.58.

*Contact author: hezhiguo@zju.edu.cn
†Contact author: meiburg@engineering.ucsb.edu

Prior studies of cohesive effects on granular collapse initially focused on dry granular columns. Mériaux and Triantafillou [23] investigated the collapse of fine powders and found that the final deposits satisfy similar scaling laws as dry noncohesive columns. Langlois *et al.* [24] conducted discrete element simulations and showed that the runout distance is greater when the cohesive blocks are highly fragmented. Additional researchers experimentally studied the collapse of wet granular media, where capillary bridges mimic a cohesive force [25–30]. Gabrieli *et al.* [26] observed the presence of clusters concentrated within the upper part of the column. Artoni *et al.* [25] found that the runout distance decreases while the final height increases with increasing cohesion. By using coarse sands, Santomaso *et al.* [27] concluded that friction remains important for irregular wet particles. Li *et al.* [29] discovered that particle size plays a dominant role in determining the flow duration of collapsing material. Wu *et al.* [30] observed that increasing the size of the column weakens the cohesion effect. Bougouin *et al.* [28] identified different regimes for cohesive granular collapse, including static, fluid-leaking, block-avalanche, and continuous-avalanche regimes. Recently, Abramian *et al.* [31] successfully estimated the macroscopic yield stress based on the cohesive contacts between grains using numerical simulations. Gans *et al.* [32] showed that the process of the cohesive granular collapse can be captured by adding a cohesive yield stress to the cohesionless granular rheological model. Staron *et al.* [33] proposed, based on numerical simulations, that stronger contact adhesion leads to weaker friction. Zhu *et al.* [34] numerically simulated submerged granular collapses and found that cohesive forces reduce the front velocity and yield a shorter and thicker final deposit compared with noncohesive submerged cases.

Our current understanding of the formation and persistence of aggregates in submerged cohesive collapses is still limited. Additionally, direct contact between particles can be significantly modified for varying packing densities. Force chains of adjacent particles that transfer force from one neighbor to the next can be very useful for describing the heterogeneous distribution of interparticle cohesive and contact forces in granular columns [35]. Many researchers have attempted to quantitatively describe force chains in granular materials [36–40]. Recently, an approach based on network science was proposed, which can automatically extract force-chain network architecture by using community detection techniques [35,41,42]. Bassett *et al.* [35] improved the community detection approach for granular materials, based on the geographical constraints that grains can only be connected to their neighbors.

In this paper, we will use the network science-based approach to examine the characteristics of cohesive and contact force chains and investigate the impact of cohesive forces and different packing densities on submerged granular collapse. To achieve this, we focus on the collapse of randomly packed submerged granular columns within a tank. The columns consist of spherical particles that are denser than the ambient fluid. To capture the microscopic details of the inter-particle forces, we employed fully coupled, grain-resolving direct numerical simulations using our in-house code PARTIES [43–45]. The introduction of the computational model can be found in the Supplemental Material [46].

In our simulation, we consider a tank of length $L \times$ height $H \times$ width $W = 100d_p \times 30d_p \times 3d_p$, with granular columns of length $L_i \times$ height $H_i = 45d_p \times 15d_p$. The granular columns are composed of spherical particles of diameter d_p. In our earlier study, we demonstrated that the size of the spanwise domain and the periodic boundaries do not exert significant influence on the process of collapse [34]. Therefore, we have chosen to set the spanwise domain size as $W = 3d_p$ and have implemented periodic boundaries in the spanwise z-direction to minimize computational costs. In the y-direction, the top surface is set to be a free-slip boundary, while no-slip boundary conditions are defined for the side walls facing the streamwise x-direction. A layer of particles with a uniform diameter of $0.5d_p$ is held fixed at the bottom boundary to mimic basal roughness. We choose the coefficients of friction and restitution as $\mu_p = 0.15$ and $e_{\text{dry}} = 0.97$, corresponding to silicate materials. The granular column is prepared via the following steps: First, the particles are randomly distributed across the entire height of the lock region. The initial particle velocity is zero, and there is no initial contact. Second, the particles settle with the friction coefficient μ_p varying from 0 to 1 to achieve different initial packing densities ϕ. Third, when all particles have settled in the lower

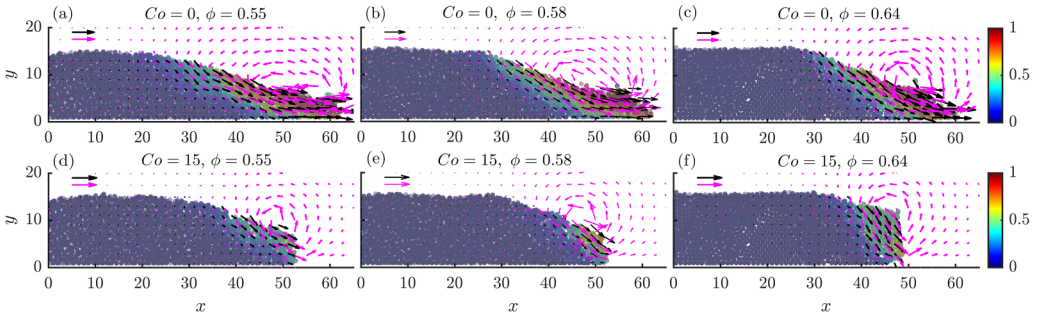

FIG. 1. Snapshots of the magnitude of the translational particle velocity $||\boldsymbol{u_p}||$ and the ambient fluid velocity $||\boldsymbol{u_f}||$ at $t = 20$ for different packing densities ϕ and cohesive numbers Co. Shown are spanwise-averaged values. The color bar shows the magnitude of the particle velocity. The black and red arrows represent vectors of the particle velocity and the fluid velocity, respectively. The horizontal arrows represent a velocity scale of 1.

part of the lock region, μ_p is adjusted back to the original value, and the collapse is initiated. The packing density of these kinds of randomly packed columns ranges from 0.55 to 0.64, which is similar to previous studies [19,22,47]. We mainly focus on the influence of the pacing density ϕ and the cohesive force strength on the granular collapse. Following Vowinckel *et al.* [44], the cohesive force in our simulations is modeled as a parabolic spring force: it is zero when two particles are in contact with each other or when the gap size ζ_n is larger than $d_p/20$. It has a maximum value when $\zeta_n = d_p/40$. All results shown below are in dimensionless form. We normalize all lengths by d_p, velocity by $u_s = \sqrt{g' d_p}$, and pressure by $\rho_f u_s^2$. Here $g' = (\rho_p - \rho_f)g/\rho_f$. ρ_p and ρ_f are the densities of the particles and the ambient fluid, respectively. g' is implemented because the reduced gravity is the primary driving force in the process of submerged granular collapse. We define the dimensionless cohesive number $Co = \max(||\boldsymbol{F}_{\text{coh}}||)/\rho_f V_p g'$ to represent the ratio of the maximum cohesive force and the characteristic gravitational force acting on a particle of volume V_p. The density ratio $r = \sqrt{\rho_p/\rho_f}$ is 1.6 and the Stokes number $St = \sqrt{\rho_p(\rho_p - \rho_f)g d_p^3}/18\sqrt{2}\nu_f\rho_f$ is 12.79, which indicates that our cohesionless cases are in the inertial regime. Here ν_f is the kinematic viscosity.

The typical submerged granular collapse includes the following stages: during the early stages, particles near the upper right of the column slide down along a concave interface that extends from the toe to the top surface of the column. As the granular flow spreads horizontally along the bottom plane, more particles within the column start to move, ultimately forming a concave deposit surface. Figure 1 illustrates snapshots of the magnitude of the translational particle velocities $||\boldsymbol{u_p}||$ and the ambient fluid velocity $||\boldsymbol{u_f}||$ in different cases. For the noncohesive loosely packed granular column, cf. Fig. 1(a), particles slide down along a concave interface and the front propagates horizontally. Large vortices form in the ambient fluid near the moving particles. With increasing packing density, fewer particles participate in the collapse process and they spread more slowly, as illustrated in Figs. 1(b) and 1(c). This observation is consistent with previous studies [19,22]. Figures 1(d)–1(f) demonstrate that the cohesive force results in more stationary particles in the lower-right part of the column. The particles propagate more slowly compared with the noncohesive cases, leading to a shorter and thicker deposit profile. A similar trend was also observed by Zhu *et al.* [34]. Cohesion also leads to a greater decrease in particle velocity for more densely packed columns. This will be explained by the following analysis of the force-chain network structure.

To examine the dilation and contraction of granular columns during the initial collapse, previous researchers calculated the change in local porosity Δn in the columns [22]. The local porosity n is calculated by subtracting the local particle volume fraction from 1. Figure 2(a) illustrates the time history of the spatially averaged change in porosity $\langle \Delta n \rangle$ in the entire column from $t = 0$ to

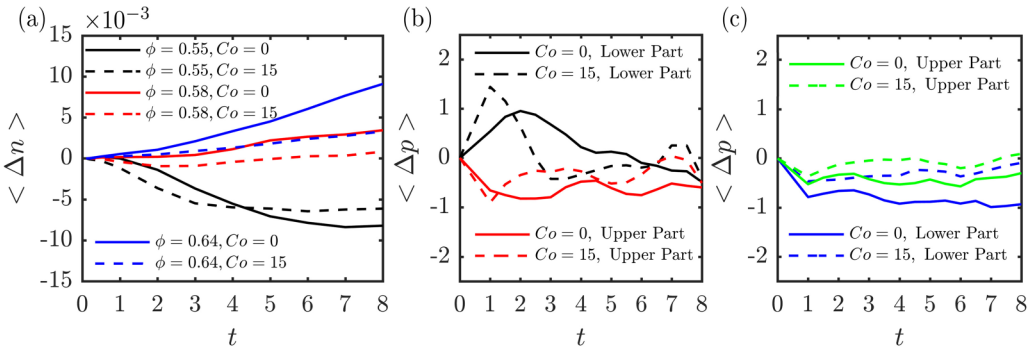

FIG. 2. Time history of the spatially averaged (a) porosity change $\langle \Delta n \rangle$ and (b), (c) excess pore pressure $\langle \Delta p \rangle$ from $t = 0$ to 8. (b) and (c) are for packing density $\phi = 0.55$ and 0.64, respectively.

8. We compute the spatial average values over all regions occupied by particles at each time unit. For loosely packed columns ($\phi = 0.55$), a contractive behavior is observed for a short time, after which the averaged porosity levels off. The cohesive force attracts particles to each other, thereby accelerating the contraction process. However, cohesion also reduces the number of collapsing particles, which limits the variation in averaged porosity. Conversely, densely packed columns ($\phi = 0.64$) exhibit a continuous expansion behavior. The cohesive force decelerates the dilation for densely packed columns. In summary, the effect of cohesion between loose and dense packing densities displays a certain asymmetry, since cohesion always tends to bring the particles closer together. In the absence of cohesion, for low-packing fractions, the tendency is for the particles to come closer together during the collapse, while for large-volume fractions, the tendency is for the particles to move farther apart. Hence for small-volume fractions, cohesion reinforces the cohesionless tendency, whereas for large-volume fractions cohesion counteracts the cohesionless tendency. At a packing density of 0.58, a value identified as critical in prior experimental studies [19], $\langle \Delta n \rangle$ exhibits a very small variation. With the effect of cohesion, $\langle \Delta n \rangle$ slightly fluctuates around zero, which indicates the granular column does not undergo significant contraction or dilation.

Figures 2(b) and 2(c) illustrate the time history of the spatially averaged excess pore pressure $\langle \Delta p \rangle$ for different a packing density ϕ and cohesive number Co. The excess pore pressure Δp is defined as the pore pressure p at each time unit minus the initial value at $t = 0$. Here we show the spatially averaged values for the upper part ($7.5 < y < 15$, $0 < x < 45$, and $0 < z < 3$) and the lower part ($0 < y < 7.5$, $0 < x < 45$, and $0 < z < 3$) of the columns, respectively. For the noncohesive loosely packed column with $\phi = 0.55$, as shown in Fig. 2(b), the initial contraction caused positive $\langle \Delta p \rangle$ in the lower part of the column, while negative $\langle \Delta p \rangle$ dominated the upper part. This qualitative observation is consistent with previous numerical findings reported by Yang *et al.* [22]. Negative $\langle \Delta p \rangle$ indicates that the interstitial fluid in the upper part of the column is more affected by the pressure reduction of the ambient fluid. As time passes, both positive and negative excess pore pressures gradually dissipate. As mentioned earlier, for the lower-packing fraction, the column initially contracts in the lower regions—i.e., the pore pressure increases to squeeze fluid out of the pore spaces. This tendency is amplified by the effects of cohesion, which want to bring the particles closer together. For the larger-packing fraction, on the other hand, the column expands everywhere—i.e., the pore pressure drops to suck fluid into the pores. This tendency is opposed by the effect of cohesion, which wants to keep the particles closer together. Consequently, this leads to a larger value of $\langle \Delta p \rangle$, as demonstrated by the dashed lines in Fig. 2(b). This can also be demonstrated by examining the standard deviations of $\langle \Delta p \rangle$ for the data in Fig. 2(b). For the upper and lower parts of the columns with $Co = 0$, the standard deviations are 0.195 and 0.463, respectively. However, when $Co = 15$, the standard deviations increase to 0.236 and 0.540.

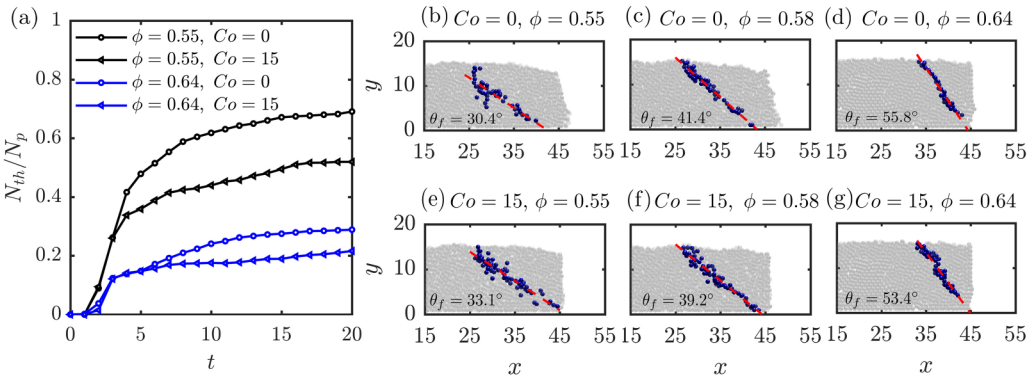

FIG. 3. (a) The evolution of the normalized number of moved particles N_{th}/N_p for different packing density ϕ and cohesive number Co. (b)–(g) The failure zones for granular columns with different Co and ϕ. The blue particles mark the failure zones and the red dashed lines are linear regressions based on the location of the failure zones.

Figure 2(c) illustrates that the initial dilation behavior in the noncohesive densely packed column with $\phi = 0.64$ induces negative excess pore pressure. Initially, a relatively small negative $\langle \Delta p \rangle$ emerges in both the upper and lower parts of the column. As time progresses, the negative $\langle \Delta p \rangle$ increases in the lower part of the column, due to the initial granular collapse. Conversely, the negative $\langle \Delta p \rangle$ gradually dissipates to zero in the upper part of the column. Similar to the changes in porosity, cohesive forces weaken the negative $\langle \Delta p \rangle$ in the densely packed column, as illustrated by the dashed lines in Fig. 2(c).

To investigate the onset of granular collapse, we located the failure zone in both time and space using a method similar to that described by Staron *et al.* [33]. We calculate the cumulative displacement of each particle relative to the initial time and identify a threshold of cumulative displacement $r_{th} = 0.2d_p$ to determine whether a particle moved or remained static. Figure 3(a) shows the evolution of the number of moved particles N_{th} over time, which is normalized by the total number of particles N_p. For noncohesive granular columns, there is a significant increase of N_{th} in a short period in the beginning, indicating the loss of stability. The apparent brief delay in the onset of collapse is due to the fact that the cumulative displacement of each particle has not yet reached the defined threshold of $0.2d_p$. At a later time, N_{th} increases slowly by the subsequent erosion process. These observations are consistent with previous simulations for dry granular collapse [33]. With the effect of the cohesive force, the failure process is of a shorter duration, and the subsequent erosion process stops sooner, which results in fewer particles being moved. This is because the cohesive force promotes the formation of aggregates and hinders the collapse of the column. Compared to loosely packed columns, densely packed columns experience fewer particle movements, and the failure process is delayed, cf. blue lines in Fig. 3(a).

We subsequently calculated the rate of change in the number of moved particles $\Delta N_{th} = N_{th}(t) - N_{th}(t-1)$ for each time unit and defined the end time of the failure process as the time t_e when ΔN_{th} has dropped to 20% of its maximum value. This approach allows us to exclude particles that propagate by subsequent erosion rather than an initial failure. To locate the failure zone, we identify the position of the particles at time t_e with a cumulative displacement ranging from $0.2d_p$ to $0.3d_p$, i.e., particles that have moved a moderate amount. Figures 3(b)–3(g) illustrate the failure zones by blue particles in various runs. Notably, we observe distinct planar failure surfaces that extend to the toe of the sliding masses. We quantify the failure surfaces in both x- and y-directions by linear regressions and calculate their angles with the horizontal, which is defined as the failure angle θ_f. For loosely packed columns, the positive excess pore fluid pressure caused by the initial contraction accelerates the particle movement, resulting in a relatively small θ_f. As

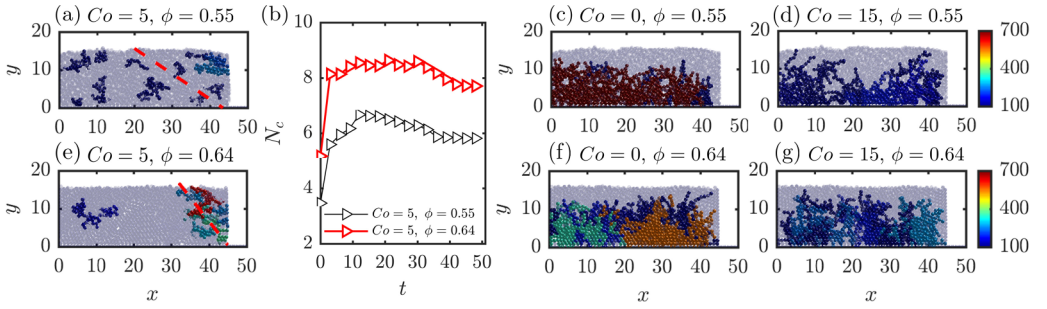

FIG. 4. (a) and (e) The community-detection results of cohesive force-chain network structures for different packing density ϕ. The red dashed lines show the failure surfaces. (b) the time history of the total number of cohesive force bonds N_c. (c), (d) and (f), (g) The community-detection results of normal contact force-chain network structures for different packing density ϕ and the cohesive number Co.

the packing density ϕ increases, fewer particles lose stability and collapse, leading to a larger θ_f. On the other hand, the failure angle θ_f evolves nonmonotonically and varies within a small range as the cohesive number Co increases. Lajeunesse *et al.* [14] found that the dry granular collapse is initiated by Mohr-Coulomb failure along a well-defined surface. The failure angle is consistent with an interpretation in terms of active Coulomb failure, which leads to a predicted failure angle $\theta_{pf} = \pi/4 + \theta_r/2$, where θ_r is the internal friction angle of the granular material. Based on previous studies of dry cohesive granular collapse [31–33], an internal friction angle of approximately 17 degrees is deemed reasonable. Thus, for a dry granular collapse, the predicted failure angle θ_{pf} is approximately 53.5 degrees. In the present study, the failure angle θ_f for submerged densely packed columns is similar to the predicted values θ_{pf}. However, θ_f for loosely packed ones is much smaller than θ_{pf}, possibly due to excess pore fluid pressure. As mentioned earlier, varying packing densities and cohesive forces have a significant impact on the internal structure of the granular columns. To understand the mechanisms behind this, it is necessary to quantitatively describe force chains, which can comprehensively explain the macroscopic collapse process from a microscopic viewpoint. We utilize the community detection algorithms [35,41,42] based on a geographical null model [35] to extract cohesive and contact force-chain network structure from the granular columns. The comprehensive derivation of the community detection approach, along with the related equations, can be found in the Supplemental Material [48] (see also references [49–51] therein).

Figures 4(a) and 4(e) compare the cohesive force-chain networks in selected granular columns. The color bar shows the number of particles S_c in each community. To investigate the onset of granular collapse, we consider the early time $t = 3$ of the failure process for each case. Here, we present the largest 10 communities to show the distribution of a strong cohesive force. In the loosely packed column with $\phi = 0.55$, cf. Fig. 4(a), the strong cohesive force chains are randomly distributed in the column. However, in the densely packed column with $\phi = 0.64$, cf. Fig. 4(e), fewer cohesive force chains are distributed in the static area. Most of the strong cohesive force chains form near the failure surface. This is because the particles in the static area of the densely packed column are in direct contact with each other and have no cohesive force between them. However, in the failure zone, small gaps form among particles due to the dilation process, which is correlated to the generation of cohesive force chains. These force chains near the failure surface present a strong macroscopic cohesive force, which opposes the collapse of the columns induced by gravity. Fig. 4(b) shows the time history of the total number of cohesive force bonds N_c for the cohesive number $Co = 5$ and different packing densities ϕ. During the evolution of the collapse process, N_c increases with time. This is a result of the formation of more cohesive force bonds when particles from the upper section descend towards the bottom. Once the particles decelerate and eventually come to a stop, they establish contact with each other, leading to a decrease in N_c until it reaches a quasi-steady value.

Figures 4(c), 4(d) and 4(f), 4(g) show the normal contact force-chain network structures in selected granular columns at $t = 1$ when the contraction or dilution process significantly impacts the distribution of contact force bonds. The communities are also characterized by their particle number S_c. Similar to the analysis of cohesive force chains, we also present the largest 10 communities to show the distribution of strong contact force. In all cases, the contact forces in the upper part of the initial columns are too weak to form multiple-particle communities, as the magnitude of the contact force depends on the weight of the overlying particles. In the lower part of the columns, the force-chain network structures of strong normal contact force are branch-like and aligned with the vertical direction, which is consistent with previous studies [22,34].

For the cohesionless loosely packed column with $\phi = 0.55$ at the beginning, the strong contact force chains cannot extend to the upper and right areas because of the initial movement of the particles in that region, cf. Fig. 4(b). As a result, the strong contact force bonds concentrate in the inner part of the column, where a large community forms and contains more than 700 particles. In the cohesive column, cf. Fig. 4(c), the size of the communities of strong contact force chains decreases significantly. Large communities are divided into several smaller ones. This can be attributed to the fact that the attractive cohesive force promotes the formation of aggregates, which results in many particles being no longer in contact with each other. As a result, only a few small communities of contact force chains form in the column. In densely packed columns with $\phi = 0.64$, more particles are in contact with each other, leading to larger communities at the beginning, as shown in Fig. 4(e). Similar to the loosely packed column, the cohesive force significantly decreases the size of the communities of strong contact force chains, cf. Fig. 4(f).

In summary, cohesion reduces the final runout distance of granular columns. It also accelerates the contraction for loosely packed columns and decelerates the dilation for densely packed columns, respectively. The planar failure surfaces of the collapsing columns have a larger angle with the horizontal plane for a higher packing density. A force-chain network analysis indicates that strong cohesive force chains are more likely to form in the failure region as the packing density increases. This induces a greater macroscopic cohesive resistance to prevent the collapse process. Additionally, we observe that the cohesive force tends to reduce the normal contact force, resulting in smaller communities of the contact force chains.

This work is supported by National Science Foundation Grant No. CBET-2138583, as well as by Grant No. W912HZ22C0037 from the U.S. Army Engineer Research & Development Center, and by Grant No. W911NF-23-2-0046 from the Army Research Office.

[1] I. V. Fine, A. B. Rabinovich, B. Bornhold, R. Thomson, and E. A. Kulikov, The Grand Banks landslide-generated tsunami of November 18, 1929: Preliminary analysis and numerical modeling, Mar. Geol. **215**, 45 (2005).

[2] R. M. Iverson, The physics of debris flows, Rev. Geophys. **35**, 245 (1997).

[3] R. M. Iverson, M. Reid, N. R. Iverson, R. LaHusen, M. Logan, J. Mann, and D. Brien, Acute sensitivity of landslide rates to initial soil porosity, Science **290**, 513 (2000).

[4] R. M. Iverson, Regulation of landslide motion by dilatancy and pore pressure feedback, J. Geophys. Res.-Earth **110**, F02015 (2005).

[5] P. H. Kuenen, Properties of turbidity currents of high density, SEPM Spec. Pub. **2**, 14 (1951).

[6] M. A. Hampton, The role of subaqueous debris flow in generating turbidity currents, J. Sediment. Res. **42**, 775 (1972).

[7] J. G. Marr, P. A. Harff, G. Shanmugam, and G. Parker, Experiments on subaqueous sandy gravity flows: The role of clay and water content in flow dynamics and depositional structures, Geol. Soc. Am. Bull. **113**, 1377 (2001).

[8] J. H. Baas, J. L. Best, and J. Peakall, Depositional processes, bedform development and hybrid bed formation in rapidly decelerated cohesive (mud–sand) sediment flows, Sedimentology **58**, 1953 (2011).
[9] G. Lube, H. Huppert, R. Sparks, and M. Hallworth, Axisymmetric collapses of granular columns, J. Fluid Mech. **508**, 175 (2004).
[10] G. Lube, H. E. Huppert, R. S. Sparks, and A. Freundt, Collapses of two-dimensional granular columns, Phys. Rev. E **72**, 041301 (2005).
[11] G. Lube, H. Huppert, R. Sparks, and A. Freundt, Static and flowing regions in granular collapses down channels, Phys. Fluids **19**, 043301 (2007).
[12] E. Lajeunesse, A. Mangeney-Castelnau, and J.-P. Vilotte, Spreading of a granular mass on a horizontal plane, Phys. Fluids **16**, 2371 (2004).
[13] N. Balmforth and R. Kerswell, Granular collapse in two dimensions, J. Fluid Mech. **538**, 399 (2005).
[14] E. Lajeunesse, J. Monnier, and G. Homsy, Granular slumping on a horizontal surface, Phys. Fluids **17**, 103302 (2005).
[15] S. Siavoshi and A. Kudrolli, Failure of a granular step, Phys. Rev. E **71**, 051302 (2005).
[16] L. Staron and E. Hinch, Study of the collapse of granular columns using two-dimensional discrete-grain simulation, J. Fluid Mech. **545**, 1 (2005).
[17] L. Lacaze and R. R. Kerswell, Axisymmetric granular collapse: A transient 3D flow test of viscoplasticity, Phys. Rev. Lett. **102**, 108305 (2009).
[18] V. Topin, Y. Monerie, F. Perales, and F. Radjai, Collapse dynamics and runout of dense granular materials in a fluid, Phys. Rev. Lett. **109**, 188001 (2012).
[19] L. Rondon, O. Pouliquen, and P. Aussillous, Granular collapse in a fluid: Role of the initial volume fraction, Phys. Fluids **23**, 073301 (2011).
[20] C. Wang, Y. Wang, C. Peng, and X. Meng, Dilatancy and compaction effects on the submerged granular column collapse, Phys. Fluids **29**, 103307 (2017).
[21] V. Topin, F. Dubois, Y. Monerie, F. Perales, and A. Wachs, Micro-rheology of dense particulate flows: Application to immersed avalanches, J. Non-Newtonian Fluid Mech. **166**, 63 (2011).
[22] G. Yang, L. Jing, C. Kwok, and Y. D. Sobral, Pore-scale simulation of immersed granular collapse: Implications to submarine landslides, JGR Earth Surface **125**, e2019JF005044 (2020).
[23] C. Mériaux and T. Triantafillou, Scaling the final deposits of dry cohesive granular columns after collapse and quasi-static fall, Phys. Fluids **20**, 033301 (2008).
[24] V. Langlois, A. Quiquerez, and P. Allemand, Collapse of a two-dimensional brittle granular column: Implications for understanding dynamic rock fragmentation in a landslide, JGR Earth Surface **120**, 1866 (2015).
[25] R. Artoni, A. C. Santomaso, F. Gabrieli, D. Tono, and S. Cola, Collapse of quasi-two-dimensional wet granular columns, Phys. Rev. E **87**, 032205 (2013).
[26] F. Gabrieli, R. Artoni, A. Santomaso, and S. Cola, Discrete particle simulations and experiments on the collapse of wet granular columns, Phys. Fluids **25**, 103303 (2013).
[27] A. Santomaso, S. Volpato, and F. Gabrieli, Collapse and runout of granular columns in pendular state, Phys. Fluids **30**, 063301 (2018).
[28] A. Bougouin, L. Lacaze, and T. Bonometti, Collapse of a liquid-saturated granular column on a horizontal plane, Phys. Rev. Fluids **4**, 124306 (2019).
[29] P. Li, D. Wang, Y. Wu, and Z. Niu, Experimental study on the collapse of wet granular column in the pendular state, Powder Technol. **393**, 357 (2021).
[30] Y. Wu, Y. Sun, and D. Wang, The combined effect of cohesion and finite size on the collapse of wet granular columns, Soft Matter **19**, 9520 (2023).
[31] A. Abramian, L. Staron, and P.-Y. Lagrée, The slumping of a cohesive granular column: Continuum and discrete modeling, J. Rheol. **64**, 1227 (2020).
[32] A. Gans, A. Abramian, P.-Y. Lagrée, M. Gong, A. Sauret, O. Pouliquen, and M. Nicolas, Collapse of a cohesive granular column, J. Fluid Mech. **959**, A41 (2023).
[33] L. Staron, L. Duchemin, and P.-Y. Lagrée, Cohesive granular columns collapsing: Numerics questioning failure, cohesion, and friction, J. Rheol. **67**, 1061 (2023).

[34] R. Zhu, Z. He, K. Zhao, B. Vowinckel, and E. Meiburg, Grain-resolving simulations of submerged cohesive granular collapse, J. Fluid Mech. **942**, A49 (2022).
[35] D. S. Bassett, E. T. Owens, M. A. Porter, M. L. Manning, and K. E. Daniels, Extraction of force-chain network architecture in granular materials using community detection, Soft Matter **11**, 2731 (2015).
[36] J. F. Peters, M. Muthuswamy, J. Wibowo, and A. Tordesillas, Characterization of force chains in granular material, Phys. Rev. E **72**, 041307 (2005).
[37] R. Arevalo, I. Zuriguel, and D. Maza, Topology of the force network in the jamming transition of an isotropically compressed granular packing, Phys. Rev. E **81**, 041302 (2010).
[38] L. Kondic, A. Goullet, C. O'Hern, M. Kramar, K. Mischaikow, and R. Behringer, Topology of force networks in compressed granular media, Europhys. Lett. **97**, 54001 (2012).
[39] S. Ardanza-Trevijano, I. Zuriguel, R. Arévalo, and D. Maza, Topological analysis of tapped granular media using persistent homology, Phys. Rev. E **89**, 052212 (2014).
[40] M. Kramár, A. Goullet, L. Kondic, and K. Mischaikow, Evolution of force networks in dense particulate media, Phys. Rev. E **90**, 052203 (2014).
[41] Y. Huang and K. E. Daniels, Friction and pressure-dependence of force chain communities in granular materials, Granular Matter **18**, 85 (2016).
[42] C. Giusti, L. Papadopoulos, E. T. Owens, K. E. Daniels, and D. S. Bassett, Topological and geometric measurements of force-chain structure, Phys. Rev. E **94**, 032909 (2016).
[43] E. Biegert, B. Vowinckel, and E. Meiburg, A collision model for grain-resolving simulations of flows over dense, mobile, polydisperse granular sediment beds, J. Comput. Phys. **340**, 105 (2017).
[44] B. Vowinckel, J. Withers, P. Luzzatto-Fegiz, and E. Meiburg, Settling of cohesive sediment: Particle-resolved simulations, J. Fluid Mech. **858**, 5 (2019).
[45] K. Zhao, B. Vowinckel, T.-J. Hsu, T. Köllner, B. Bai, and E. Meiburg, An efficient cellular flow model for cohesive particle flocculation in turbulence, J. Fluid Mech. **889**, R3 (2020).
[46] See Supplemental Material at http://link.aps.org/supplemental/10.1103/PhysRevFluids.9.084302 for the introduction of the computational model.
[47] X. Chateau, Particle packing and the rheology of concrete, in *Understanding the Rheology of Concrete* (Elsevier, 2012), pp. 117–143.
[48] See Supplemental Material at http://link.aps.org/supplemental/10.1103/PhysRevFluids.9.084302 for the comprehensive derivation of the community detection approach and the related equations, which includes Refs. [49–51].
[49] S. Mandal, M. Nicolas, and O. Pouliquen, Insights into the rheology of cohesive granular media, Proc. Natl. Acad. Sci. USA **117**, 8366 (2020).
[50] S. Fortunato, Community detection in graphs, Phys. Rep. **486**, 75 (2010).
[51] L. G. S. Jeub, M. Bazzi, I. S. Jutla, and P. J. Mucha, A generalized Louvain method for community detection implemented in MATLAB, https://github.com/GenLouvain/GenLouvain (2011–2019).